ELSEVIER

Contents lists available at ScienceDirect

Solid State Sciences

journal homepage: www.elsevier.com/locate/ssscie





Luminescence of alkali rare earth borates $A_3Ln(BO_3)_2$ (A = Na, K; Ln = Eu, Tb)

Adrian T. Hines ^{a,b}, Gregory Morrison ^{a,b}, Brandon J. Yarbrough ^{a,b}, Natalia B. Shustova ^{a,b}, Luiz G. Jacobsohn ^c, Hans-Conrad zur Loye ^{a,b,*}

- ^a Center for Hierarchical Waste Form Materials, Columbia, SC, 29208, United States
- b Department of Chemistry and Biochemistry, University of South Carolina, Columbia, SC, 29208, United States
- ^c Department of Materials Science and Engineering, Clemson University, Clemson, SC, 29634, United States

ARTICLE INFO

Keywords: Borates Flux crystal growth Photoluminescence Radioluminescence

ABSTRACT

Single crystals of a series of rare earth borates, A_3Ln (BO₃) (A = Na, K; Ln = Eu, Tb), were synthesized using a boric acid/hydroxide melt. The Na₃Ln (BO₃)₂ borates crystallized in the monoclinic system with space group $P2_1/n$, and the K₃Ln (BO₃)₂ borates crystallized in the orthorhombic system with space group *Pnma*. The luminescence of these borates was investigated under ultraviolet and X-ray excitations for the first time. Radioluminescence (RL) measurements showed K₃Tb(BO₃)₂ to be the brightest compound, with an integral intensity equal to 55% of the integral emission of Bi₄Ge₃O₁₂ (BGO) powder.

1. Introduction

Luminescence is a relevant functionality in many technologies, from lighting to medical imaging and sensing. Luminescent materials can be excited in different ways, including ultraviolet (UV) light and X-rays, and borates are of interest as host lattices for phosphors due to their large bandgap, chemical and thermal stabilities, broad UV transparency, and the structural diversity afforded to them by the $B_x O_y$ building units. Elements such as rare earths are particularly useful in designing luminescent materials and, therefore, the combination of these components in one material can result in promising functionalities. Many doped and self-activated luminescent borates exist, including (Y, Gd, Lu)BO_3:Eu^3+ [1], SrB_4O_7:Ln^2+ [2], LiY(BO_3):Eu^3+ [3], Ba_3YB_9O_{18} [4], Ln (BO_3) (Ln = Nd, Eu, Gd, Tb) [5], MgB_4O_7:Ce, Li [6], as well as borate glasses [7–9], thus making the exploration of rare earth borates a promising research area.

Materials that luminesce under ionizing radiation have potential for use as radiation detection devices to check for the presence of nuclear materials. In this regard, the relatively high concentration of boron in these compounds may be of interest to neutron detection. The crystal growth of these borate materials was achieved via high temperature flux growth, an approach that has proven to be an efficient strategy for the discovery of new materials in single crystal form [10–14]. These crystals are reasonably sized (1 mm) for exploratory purposes. The fact that

these borates readily form as crystals suggests that large crystal growth could be achieved in the future. Herein, we report on the investigation of the luminescence of several alkali rare earth borates, namely Na₃Tb (BO₃)₂, K₃Tb(BO₃)₂, Na₃Eu(BO₃)₂, and K₃Eu(BO₃)₂, under UV and X-ray excitation.

2. Experimental procedure

Prior to use, Tb₄O₇ (Alfa Aesar, 99.99%) was reduced to Tb₂O₃ by heat-treatment at 1000 °C under H₂/N₂ gas flow. Crystals of A₃Ln (BO₃)₂ (A = Na, K; Ln = Eu, Tb) were obtained by placing 1.0 mmol of Ln₂O₃ inside silver tubes and covering them with 5 g of NaOH:H₃BO₃ (NaOH: H₃BO₃) in an 80:20 mass ratio. The tubes were crimped shut, heated to 250 °C at a rate of 120 °C/h and held at that temperature for 1 h, heated to 650 °C for Eu and 750 °C for Tb for 12 h and slow cooled to 100 °C at 6 °C/h. The samples were removed from the silver tubes and washed with water to remove the flux and isolate the reaction products.

2.1. Characterization

The purity of ground samples was confirmed on picked single crystals using powder X-ray diffraction. Diffraction data were collected on a Bruker D2 Phaser equipped with a Cu K α source (= 1.54018 Å). Powder diffraction data are provided in Figs. S1–S4 of the supporting

^{*} Corresponding author. Center for Hierarchical Waste Form Materials and Department of Chemistry and Biochemistry, Columbia, SC, 29298, United States. E-mail address: zurloye@mailbox.sc.edu (H.-C. zur Loye).

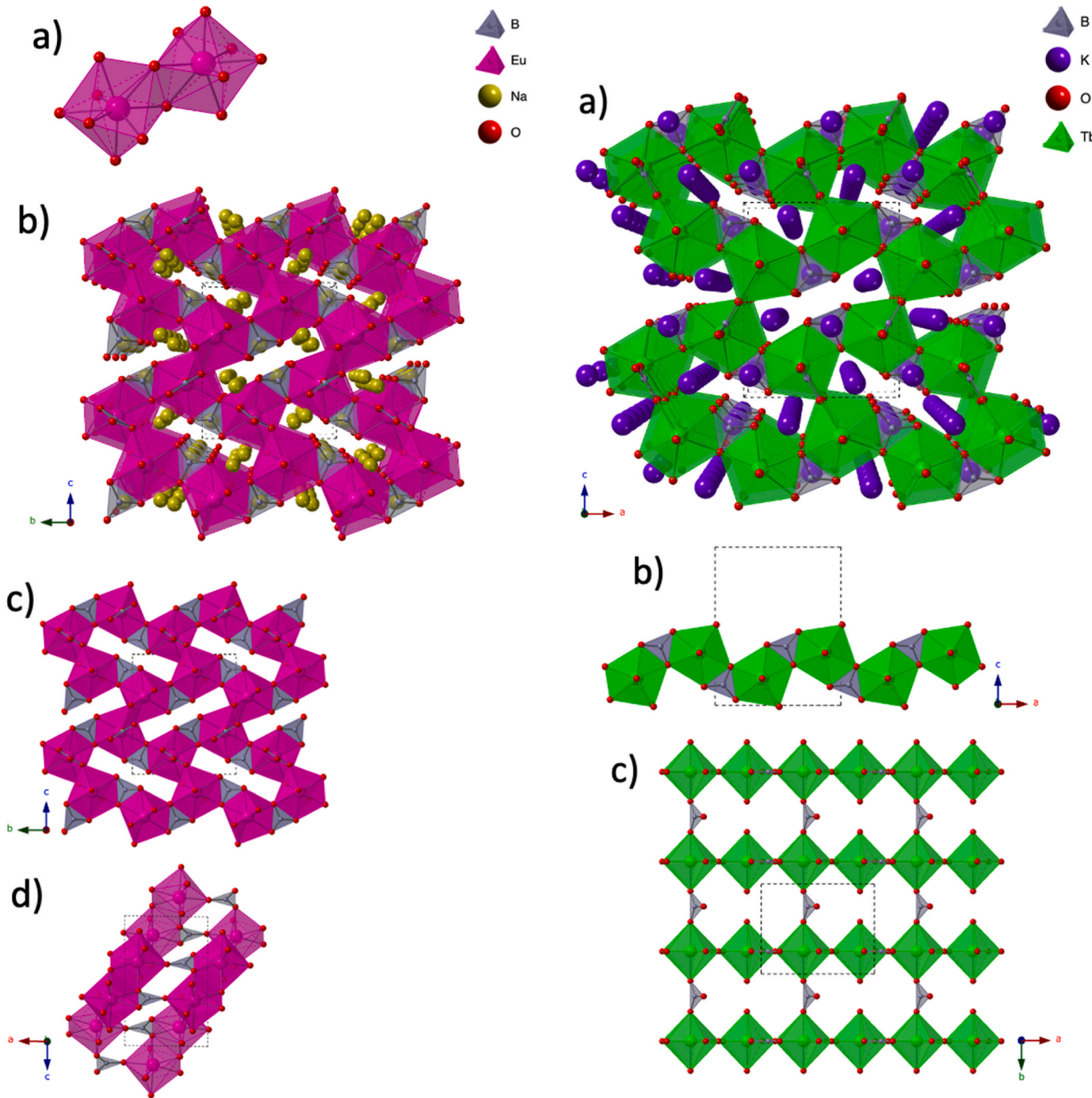


Fig. 1. (a) EuO $_8$ polyhedra edge-share oxygen to form (b) stacked layers of LnO $_8$ units with sodium cations in the void spaces (c) EuO $_8$ layer containing BO $_3$ trigonal planar units and (d) sheets connected to adjacent sheets via BO $_3$ units. EuO $_8$ polyhedra are pink, boron polyhedra grey, sodium gold, and oxygen red.

information.

Photoluminescence (PL) spectra were collected on single crystals of $Na_3Eu(BO_3)_2$, $Na_3Tb(BO_3)_2$, $K_3Eu(BO_3)_2$, and $K_3Tb(BO_3)_2$ using a Horiba Micro-SPEX system equipped with a Horiba iHR320 imaging spectrograph and a Syncerity CCD detector. Excitation was provided by a confocal 375 nm diode laser. Data were collected using Labspec 6 in the range of 400–800 nm with a laser excitation source power of 0.4 mW and a 10X UV objective.

Fig. 2. (a) Full structure image of K_3Ln (BO₃)₂ showing infinite layers with potassium ions in the voids (b) infinite chain of $[LnO_4BO_3]_8^{B_-}$ (c) framework diagram of K_3Ln (BO₃)₂ (Ln = Eu, Tb). TbO₇ polyhedra are light green, boron polyhedra grey, potassium polyhedra purple, and oxygen red.

Radioluminescence (RL) measurements were obtained using a Freiberg Instruments Lexsyg spectrofluorometer equipped with a Varian Medical Systems VF-50J X-ray tube with a tungsten anode. To achieve continuous radiation intensity monitoring, the X-ray source was coupled with a Crystal Photonics CXD-S10 photodiode. Scintillation of the sample was measured using an Andor Technology SR-OPT-8024 optical fiber connected to an Andor Technology Shamrock 163 spectrograph coupled to a cooled (–80 °C) Andor Technology DU920P-BU Newton CCD camera (spectral resolution of ~0.5 nm/pixel). The powdered samples filled ~8 mm diameter, 0.5 mm deep cups thus allowing for

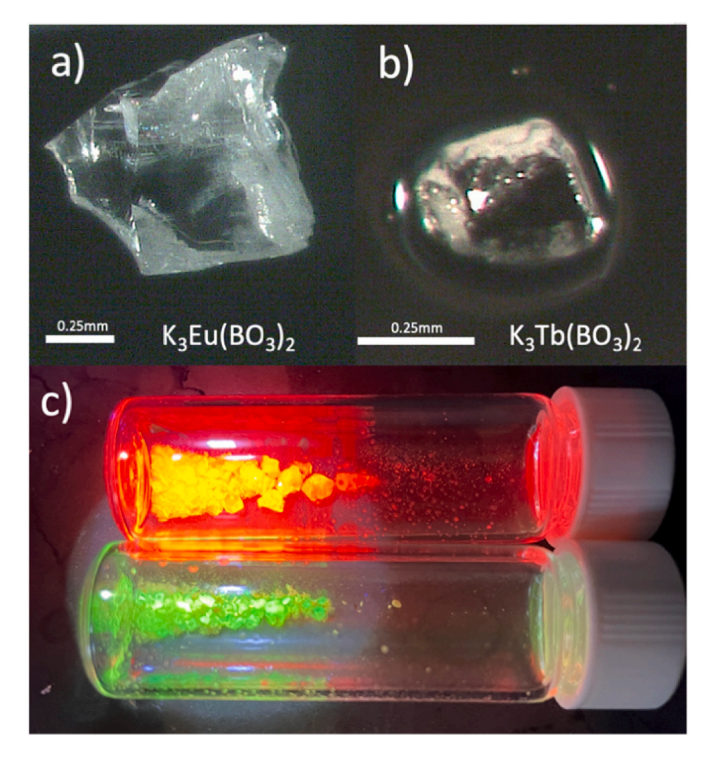


Fig. 3. Crystal images of (a) K₃Eu(BO₃)₂, (b) K₃Tb(BO₃)₂, and (c) of them (top and bottom, respectively) under UV excitation.

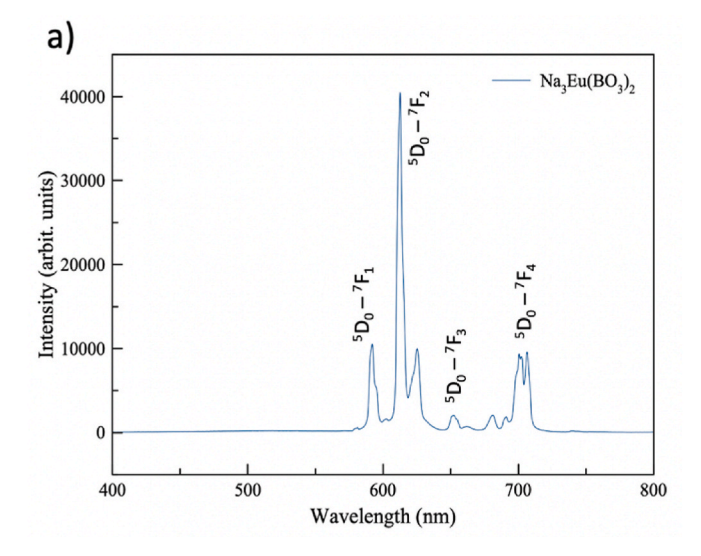
comparison of relative intensities, while bismuth germanium oxide (BGO) powder (Alfa Aesar Puratronic, 99.9995% (metals basis)) was used as a reference. RL was measured under continuous X-ray irradiation (40 kV, 1 mA) with integration time of 1 s. Spectra were automatically corrected using the spectral response of the system determined by the manufacturer.

3. Results and discussion

3.1. Structure description

Briefly, Na₃Ln (BO₃)₂ (Ln = Eu, Tb) crystallizes in the monoclinic system with space group $P2_1/n$ [10]. The framework structure consists of Ln₂O₁₄ dimers that are constructed from LnO₈ polyhedra. These units are joined through two apical oxygens to two adjacent LnO₈ polyhedra, forming a sheet in the b-direction. The polyhedra within the sheets are reinforced via BO₃ trigonal planar units in the b-direction and, furthermore, the individual sheets are connected to adjacent sheets via BO₃ linking groups in the c-direction, shown in Fig. 1. The sodium cations are located in the void spaces within the framework. There is only one crystallographic site for the rare earths.

 $K_3Ln~(BO_3)_2~(Ln=Eu,Tb)$ crystallizes in the orthorhombic system with space group *Pnma*. The framework structure consists of LnO_7 polyhedra linked together through trigonal planar borate units, with potassium ions located within the channels of the structure. The LnO_7 polyhedra are connected via equatorial oxygen to form infinite chains in the bc plane. The chains are reinforced via BO_3 trigonal planar units to form $[LnBO_6]_6^{6-}$ chains that are linked to adjacent chains through BO_3 units, shown in Fig. 2. The K^+ ions are located in the void space between



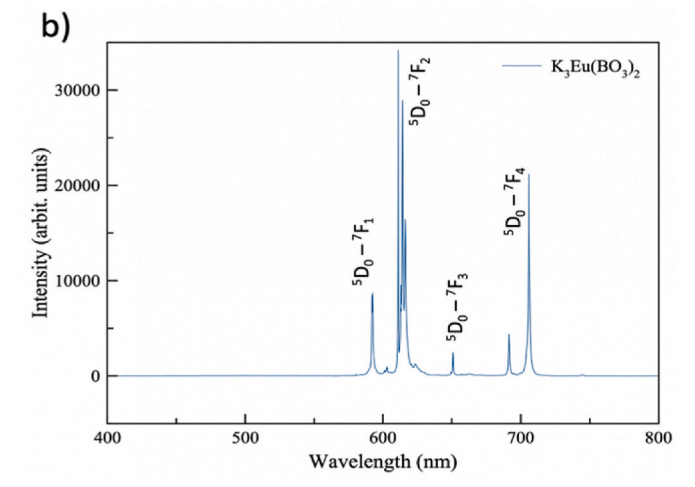
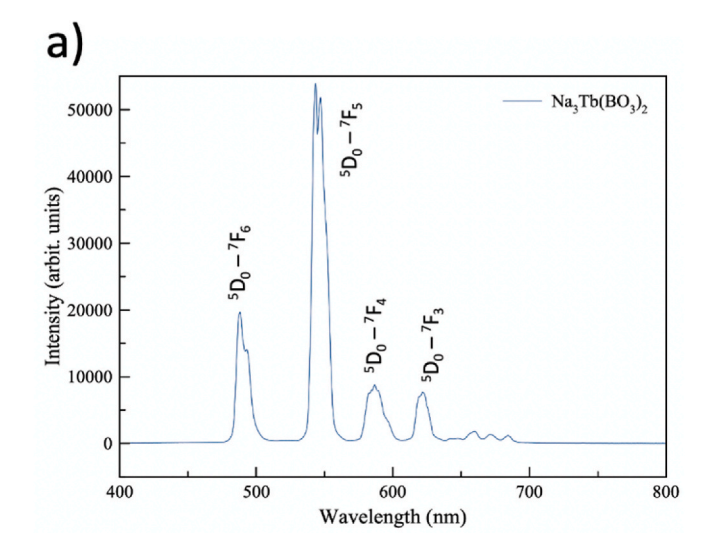


Fig. 4. Emission spectra of (a) $Na_3Eu(BO_3)_2$ and (b) $K_3Eu(BO_3)_2$ measured at room temperature under 375 nm excitation.

the chains. There is only one crystallographic site for the rare earths.

3.2. Luminescence properties

Typical crystals of $K_3Eu(BO_3)_2$ and $K_3Tb(BO_3)_2$ are shown in Fig. 3, along with their UV-excited red and green luminescence, respectively. Excitation spectra for all compounds are provided in Figs. S5–S8 of the supplemental information. The PL emission spectra of $Na_3Tb(BO_3)_2$ and $K_3Tb(BO_3)_2$, and $Na_3Eu(BO_3)_2$, and $K_3Eu(BO_3)_2$ single crystals measured at room temperature are shown in Figs. 4 and 5, respectively. The luminescence spectra are composed by a series of sharp lines corresponding to the 4*f*-4*f* electronic transitions of Eu^{3+} (Fig. 4) and Tb^{3+} (Fig. 5), as indicated in the figures. The emission spectra for $Na_3Eu(BO_3)_2$, and $K_3Eu(BO_3)_2$ are dominated by two strong emission peaks at 590 and 612 nm corresponding to the $^5D_0 \rightarrow ^7F_1$ and $^5D_0 \rightarrow ^7F_2$ transitions, respectively. Generally, insight into the site symmetry of Eu^{3+} can be obtained from the intensities of the $^5D_0 - ^7F_J$ emissions. When Eu^{3+} ions are located on a site with inversion symmetry, the $^5D_0 \rightarrow ^7F_1$



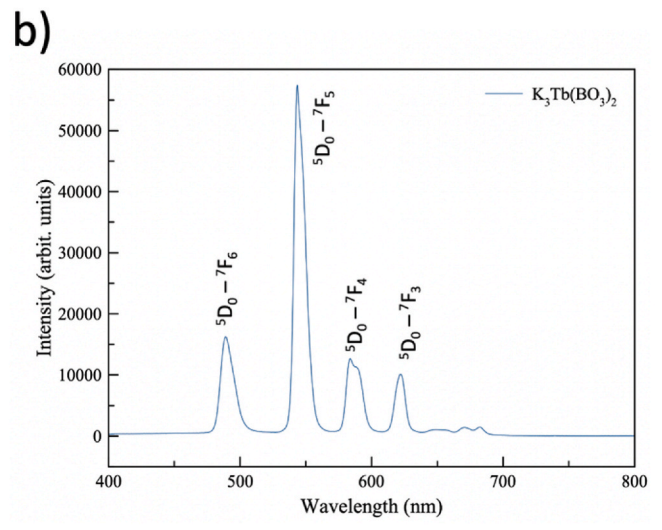
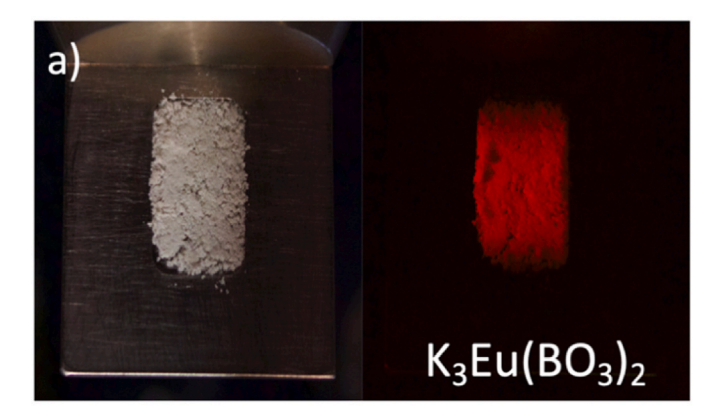


Fig. 5. Emission spectra of (a) $Na_3Tb(BO_3)_2$ and (b) $K_3Tb(BO_3)_2$ at room temperature under 375 nm excitation.

magnetic dipole transition is allowed and the emission peak at 590 nm dominates the spectra. In contrast, if the ${\rm Eu}^{3+}$ ions occupy sites that do not possess inversion symmetry, the 5d configurations are mixed into $4f^n$ electron configurations. As a result of the inversion symmetry being broken, the $^5D_0 \rightarrow ^7F_2$ electric dipole transition is no longer forbidden and becomes the most intense, resulting in the dominant emission peak at 612 nm [15–18]. This is the case for Na₃Eu(BO₃)₂ and K₃Eu(BO₃)₂, where the Eu $^{3+}$ ions are located on sites in the structure that do not possess inversion symmetry.

For the Tb analogues, the strong emission peaks are centered at 482 nm, 537 nm, 578 nm, 612 nm and are a result of the $^5D_4 \rightarrow ^7F_6, ^5D_4 \rightarrow ^7F_5, ^5D_4 \rightarrow ^7F_4, ^5D_4 \rightarrow ^7D_3$ transitions, respectively, shown in Fig. 5. No luminescence was observed below the $^5D_4 \rightarrow ^7F_6$ transition down to 400 nm, suggesting that radiative $^5D_3 \rightarrow ^7F_J$ transitions do not occur. In other known luminescent compounds containing Tb $^{3+}$ [19,20], the maximum emission peak occurs between 536 nm and 558 nm (green region). Both Na₃Tb(BO₃)₂ and K₃Tb(BO₃)₂ reported herein show a maximum emission peak at 550 nm, in agreement with previous results.



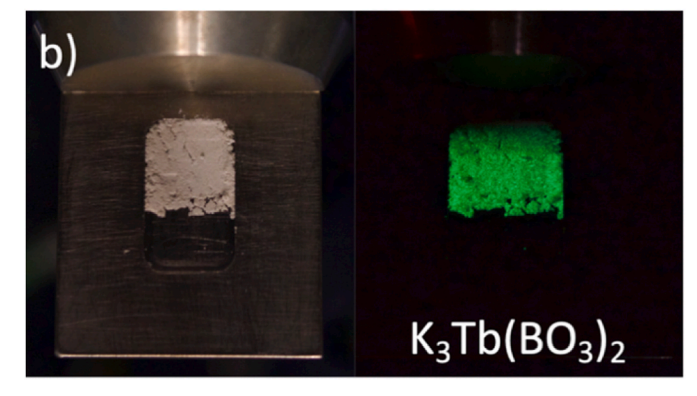


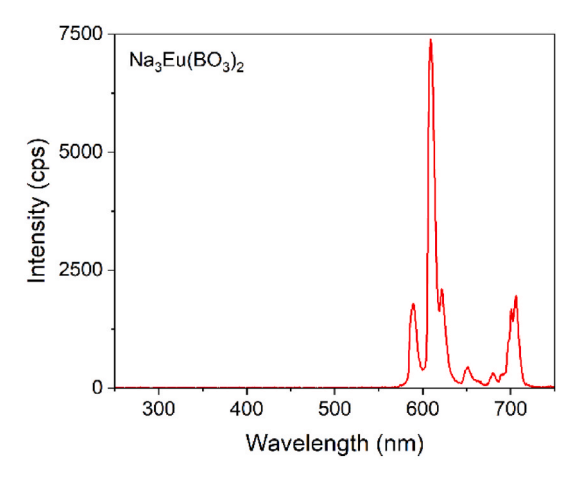
Fig. 6. Powdered sample (left) and its respective radioluminescence under X-ray irradiation (right) of (a) K₃Eu(BO₃)₂ and (b) K₃Tb(BO₃)₂.

The luminescence of these borates was also investigated under X-ray excitation. Fig. 6 illustrates the radioluminescence emission of K_3Eu (BO₃)₂ and $K_3Tb(BO_3)_2$ powders with images taken with a digital camera inside a Rigaku Ultima IV diffractometer operated with a Cu K α source ($\lambda=1.54018$ Å). The red and green colors are typical of Eu^{3+} and Tb^{3+} activators, respectively.

Radioluminescence spectra of Na₃Eu(BO₃)₂, K₃Eu(BO₃)₂, Na₃Tb (BO₃)₂, and K₃Tb(BO₃)₂ in powder form are shown in Figs. 7 and 8 for the Eu and Tb compounds, respectively. The spectra of Na₃Eu(BO₃)₂ and K₃Eu(BO₃)₂ are dominated by the sharp emission centered at 610 nm characteristic of 4*f*-4*f* Eu³⁺ transitions in sites lacking inversion symmetry, as discussed above. These results are consistent with the PL measurements and revealed the Eu borates to be free of additional emission bands that could potentially originate from intrinsic defects.

The spectra of the Tb borates, $Na_3Tb(BO_3)_2$ and $K_3Tb(BO_3)_2$, are dominated by the emission line centered at 540 nm characteristic of 4f-4f Tb³⁺ transitions as shown in Fig. 8. As in the case of the Eu borates, these results are consistent with the respective PL measurements and revealed the Tb borates to be free of additional emission bands or intrinsic defects.

Radioluminescence measurements were also used to estimate the relative brightness against commercial $Bi_4Ge_3O_{12}$ (BGO) powder. These results are shown in Fig. 9 where the integral emission between 300 and 750 nm of all samples was determined. These measurements revealed that $K_3Tb(BO_3)_2$ was the brightest presenting 55% of the integral emission of the BGO powder at room temperature.



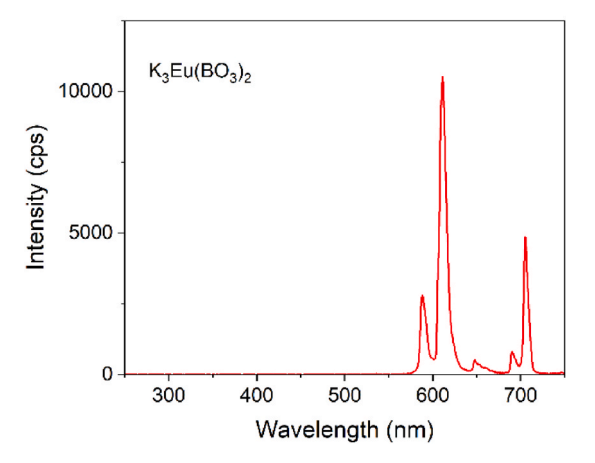


Fig. 7. Radioluminescence spectra of $Na_3Eu(BO_3)_2$ (left) and $K_3Eu(BO_3)_2$ (right) measured at room temperature.

4. Conclusions

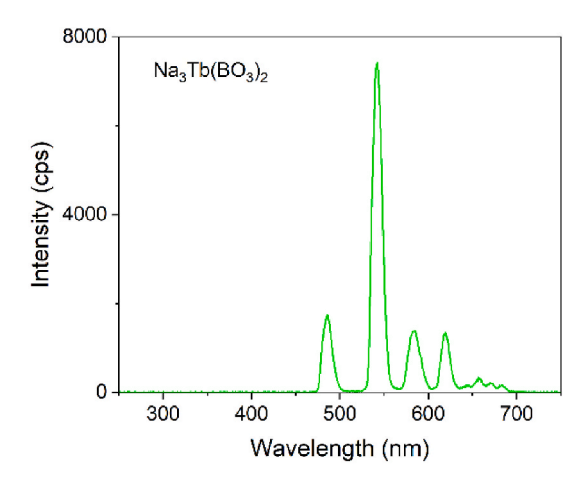
Crystals of Na₃Eu(BO₃)₂, K₃Eu(BO₃)₂, Na₃Tb(BO₃)₂, and K₃Tb(BO₃)₂ were synthesized using a molten hydroxide/boric acid melt and their luminescence properties were investigated. The Na₃Ln (BO₃)₂ borates crystallized in the monoclinic system with space group $P2_1/n$, and the K₃Ln (BO₃)₂ borates crystallized in the orthorhombic system with space group *Pnma*. The luminescence of all borates was investigated under UV and X-ray excitation, with their emission spectra being characteristic of the rare earth element that is present in the structure. K₃Tb(BO₃)₂ was the brightest material with its integral emission reaching 55% of BGO powder at room temperature. No emission from defects or impurities was observed. This work confirms that the investigation of borates offers many opportunities for the discovery of new luminescent and scintillating materials.

Accession codes

CCDC 2161519, 2161521, 2164464, 2161818 contain the supplementary crystallographic data for this paper. These data can be obtained free of charge via www.ccdc.cam.ac.uk/data_request/cif, or by emailing data_request/cif, or by contacting The Cambridge Crystallographic Data Center, 12 Union Road, Cambridge CB2 1EZ, UK; fax: +44 1223 336033.

Declaration of competing interest

The authors declare that they have no known competing financial



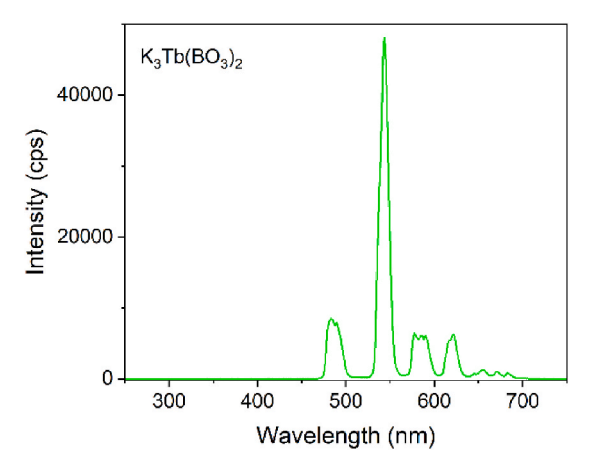


Fig. 8. Radioluminescence spectra of $Na_3Tb(BO_3)_2$ (left) and $K_3Tb(BO_3)_2$ (right) measured at room temperature.

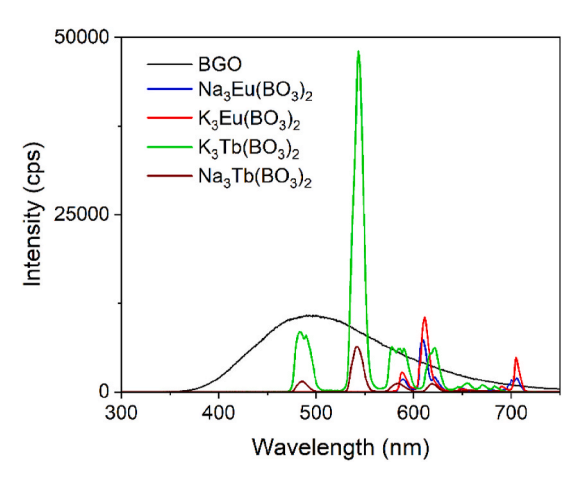


Fig. 9. Radioluminescence output comparison of all four borates and commercial BGO powder.

interests or personal relationships that could have appeared to influence the work reported in this paper.

Data availability

Data will be made available on request.

Acknowledgements

Research was conducted by the Center for Hierarchical Waste Form Materials (CHWM), an Energy Frontier Research Center (EFRC). Research was supported by the U.S. Department of Energy, Office of Basic Energy Sciences, Division of Materials Sciences and Engineering, under Award DE-SC0016574. L.G. Jacobsohn acknowledges support by the National Science Foundation under Grant No. 1653016 for collecting and analyzing the radioluminescence spectra.

Appendix A. Supplementary data

Supplementary data to this article can be found online at https://doi.org/10.1016/j.solidstatesciences.2023.107130.

References

- [1] L. Chen, Y. Jiang, G. Yang, G. Zhang, X. Xin, D. Kong, J. Rare Earths 27 (2009) 312–315.
- [2] R. Stefani, A.D. Maia, E.E.S. Teotonio, M.A.F. Montiero, M.C.F.C. Felinto, H. F. Brito, J. Solid State Chem. 179 (2006) 1086–1092.
- [3] G. Ju, Y. Hu, H. Wu, Z. Yang, C. Fu, Z. Mu, F. Kang, Opt. Mater. 33 (2011) 1297–1301.
- [4] M. He, X.L. Chen, Y.P. Sun, J. Liu, J.T. Zhao, C.J. Duan, Cryst. Growth Des. 7 (2007) 199–201.
- [5] G. Jia, H. You, M. Yang, L. Zhang, H. Zhang, J. Phys. Chem. C 113 (2009) 16638–16644.

- [6] T.D. Gustafson, E.D. Milliken, L.G. Jacobsohn, E.G. Yukihara, J. Lumin. 212 (2019) 242–249.
- [7] I.J. Tillman, M.A. Dettmann, V.V. Herrig, Z.L. Thune, A.J. Zieser, S.F. Michalek, M. O. Been, M.M. Martinez-Szewczyk, H.J. Koster, C.J. Wilkinson, M.W. Kielty, L. G. Jacobsohn, U. Akgun. Opt. Mater. 68 (2017) 58–62.
- [8] L. Pan, J.K.M.F. Daguano, N.M. Trindade, M. Cerruti, E.D. Zanotto, L.G. Jacobsohn, Opt. Mater. 104 (2020), 109847.
- [9] M.W. Kielty, M. Dettmann, V. Herrig, M.G. Chapman, M.R. Marchewka, A. A. Trofimov, U. Akgun, L.G. Jacobsohn, J. Non-Cryst. Solids 471 (2017) 357–361.
- [10] A.T. Hines, G. Morrison, H.B. Tisdale, M.D. Smith, T.M. Besmann, A. Mofrad, M. Aziziha, R.E. Booth, K. Sun, G.S. Was, H.-C. zur Loye, Inorg. Chem. 61 (2022) 11232–11242.
- [11] A.M. Latshaw, W.M. Chance, N. Trenor, G. Morrison, M.D. Smith, J. Yeon, D. E. Williams, H.-C. zur Loye, CrystEngComm 17 (2015) 4691–4698.
- [12] A.M. Latshaw, G. Morrison, K.D. zur Loye, A.R. Myers, M.D. Smith, H.-C. zur Loye, CrystEngComm 18 (2016) 2294–2302.
- [13] D. Carone, V.V. Klepov, J.C. Schaeperkoetter, S.T. Misture, L.G. Jacobsohn, M. Aziziha, J. Schorne-Pinto, S.A.J. Thomason, A.T. Hines, T.M. Besmann, H.-C. zur Loye, Inorganics 10 (2022) 83.
- [14] D. Carone, L.G. Jacobsohn, L.S. Breton, H.-C. zur Loye, Solid State Sci. 127 (2022),
- [15] A.O. Wright, M.D. Seltzer, J.B. Gruber, B.H.T. Chai, J. Appl. Phys. 78 (1995) 2456.
- [16] I.P. Sahu, D.P. Bisen, N. Brahme, R.K. Tamrakar, J. Radiat. Res. Appl. Sci. 8 (2015) 104–109.
- [17] J. Zhong, X. Ming, D. Chen, G. Xiao, Z. Ji, Dyes Pigments 146 (2017) 272-278.
- [18] X. Huang, G. Heng, L. Bin, J. Alloys Compd. 720 (2017) 29-38.
- [19] J.C.A. Santos, E.P. Silva, N.R.S. Souza, Y.G.S. Alves, D.V. Sampaio, C. Kucera, L. G. Jacobsohn, J. Ballato, R.S. Silva, Ceram. Int. 45 (2019) 3797–3802.
- [20] R.E. Muenchausen, L.G. Jacobsohn, B.L. Bennett, E.A. McKigney, J.F. Smith, J. A. Valdez, D.W. Cooke, J. Lumin. 126 (2007) 838–842.